Eurasian Journal of Physics and Functional Materials

Volume 8 | Number 3

Article 3

Pages: 111 - 121

2024

RF sputtered in-plane NiO-based lithium-metal microbattery

Yer-Targyn Tleukenov
National Laboratory Astana, Nazarbayev University, Kabanbay Batyr Ave. 53, Astana 010000, Kazakhstan

Mukagali Yegamkulov
National Laboratory Astana, Nazarbayev University, Kabanbay Batyr Ave. 53, Astana 010000, Kazakhstan

Yessimzhan Raiymbekov
National Laboratory Astana, Nazarbayev University, Kabanbay Batyr Ave. 53, Astana 010000, Kazakhstan

Arailym Nurpeissova
National Laboratory Astana, Nazarbayev University, Kabanbay Batyr Ave. 53, Astana 010000, Kazakhstan

Zhumabay Bakenov
National Laboratory Astana, Nazarbayev University, Kabanbay Batyr Ave. 53, Astana 010000, Kazakhstan

See next page for additional authors

Recommended Citation

Tleukenov, Yer-Targyn; Yegamkulov, Mukagali; Raiymbekov, Yessimzhan; Nurpeissova, Arailym; Bakenov, Zhumabay; and Mukanova, Aliya (2024) "RF sputtered in-plane NiO-based lithium-metal microbattery," *Eurasian Journal of Physics and Functional Materials*: Vol. 8: No. 3, Article 3.
DOI: https://doi.org/10.69912/2616-8537.1226

RF sputtered in-plane NiO-based lithium-metal microbattery

Authors

Yer-Targyn Tleukenov, Mukagali Yegamkulov, Yessimzhan Raiymbekov, Arailym Nurpeissova, Zhumabay Bakenov, and Aliya Mukanova

ORIGINAL STUDY

RF Sputtered In-plane NiO-based Lithium-metal Microbattery

Yer-Targyn Tleukenov [a], Mukagali Yegamkulov [a], Yessimzhan Raiymbekov [a], Arailym Nurpeissova [a,b,c], Zhumabay Bakenov [a,b,c,*], Aliya Mukanova [a,b,c,**]

[a] National Laboratory Astana, Nazarbayev University, Kabanbay Batyr Ave. 53, Astana 010000, Kazakhstan
[b] Institute of Batteries LLC, Kabanbay Batyr Ave. 53, Astana 010000, Kazakhstan
[c] Department of Chemical and Materials Engineering, School of Engineering and Digital Sciences, Nazarbayev University, Kabanbay Batyr Ave. 53, Astana 010000, Kazakhstan

Abstract

The goal to further increase energy and power density of conventional two-dimensional (2D) structured lithium-ion batteries (LIBs) is driving research towards more complex three-dimensional (3D) batteries with large surface area and accordingly high active material mass loading. So far, many attempts have been implemented to prepare 3D structured LIBs. A highly developed 3D surface allows for a larger amount of active material to be deposited while maintaining a smaller thickness, thus avoiding the challenges associated with a thick electrode. Herein, this paper presents development of in-plane type 3D NiO thin film electrodes produced by radio frequency (RF) magnetron sputtering. The physico- and electro-chemical properties were studied depending on the post-annealing temperature which was in the range of 200−300 °C. It was shown that an in-plane NiO thin film anode with GPE can be developed to enable battery operation without the use of a commercial separator. As a gel-polymer electrolyte (GPE) was used poly(ethylene oxide)-poly(vinylidene fluoride) (PEO-PVDF-co-HFP). The in-plane 3D battery with PEO-PVDF-co-HFP GPE exhibited outstanding cycling stability of 60 cycles, delivering a capacity of 510 mAh g^{-1}. The developed 3D battery, as a result, demonstrated improved cycling stability and electrochemical performance while effectively operating at 0.1C rate.

Keywords: Nickel oxide (NiO), Thin film, In-plane, Lithium-metal, Microbattery, 3D, Sputtering, Gel polymer electrolyte (GPE)

1. Introduction

The demand for lithium-ion batteries (LIBs) has recently been rising quickly due to the rapid development of wireless high tech devices, such as portable electronics, electric vehicles, and the growing need to store new green energy (solar, tide energy, wind, nuclear, biomass, etc.) in smart grids [22−24].

The possibility of employing transition metal oxides (Zn, Co, Ni, Mn, Cu, Mo, Sn, etc.) as anode materials in LIBs has recently been the subject of numerous investigations. Due to their specific capacity, which is two to three times more than that of graphite, transition metal oxides are drawing interest for this application. They are now employed as anode materials for conventional LIBs [1−15]. NiO, ZnO, and SnO_2 have a high theoretical capacity and a high lithium-ion diffusion coefficient when utilized as anode materials for LIBs [18−21]. Among the different transition metal oxides, NiO stands out for their affordability, ease of production, chemical stability, and high exciton binding energy [16,17].

Despite having high specific capacities electrodes have several limitations that prevent widespread use. As the charge/discharge cycle advances, the significant volume changes during the lithiation and delithiation processes limit the stability of the specific capacity due to their low electrical conductivity. Low cell voltage caused by the high delithiation potential results in a significantly lower energy density compared to cells

Received 3 June 2024; revised 20 September 2024; accepted 3 September 2024.
Available online 19 October 2024

* Corresponding author.
** Corresponding author.
E-mail addresses: zbakenov@nu.edu.kz (Z. Bakenov), aliya.mukanova@nu.edu.kz (A. Mukanova).

https://doi.org/10.69912/2616-8537.1226

with graphite anodes. The extreme polarization causes the charge transfer kinetics to be poor, which results in low energy efficiency. Another major difficulty is the low coulombic efficiency (CE) of conversion-type anodes, particularly in the first cycle. A battery's overall cost rises as a result of the anode's initial low coulombic efficiency, which increases the consumption of electrolyte and cathode materials. The substantial irreversible capacity brought on by the creation of solid electrolyte interphase (SEI) in the initial discharge process is a fundamental factor in the low initial coulombic efficiency of nanostructured electrode material [34]. Particularly for electrodes based on conversion processes and alloying/dealloying, the first lithiation of an electrode is always accompanied by a dramatic volume expansion of the electrode material. The enormous irreversible capacity and low initial coulombic efficiency would result from the large volume expansion and alternate fracture, which would occur if the potential range of the SEI production overlaps with that of lithiation processes. In contrast to Li/Li^+, the initial discharge plateau of NiO electrodes is consistently found between 0.5 and 0.7 V [5–15], which meet the potential for the creation of the SEI [16,17]. According to this, reducing the co-occurrence of the lithiation reaction and the SEI production should be a workable solution to the low initial coulombic efficiency of the NiO electrode.

The microstructure and morphological characteristics of oxide electrodes have a significant impact on their electrochemical performance. Nanostructured NiO electrodes continuously demonstrate enhanced electrochemical performance, whereas bulk NiO anodes displayed very low rate performance and poor cyclability (188 $mAgh^{-1}$ at 0.1 C after 50 cycles) (29 $mAgh^{-1}$ at 2C) [33]. Many research groups have moved their focus to improving power density to fulfill the performance needs of some emerging sophisticated applications [25–27]. In order to get a high energy density for batteries, the electrode surface area may be increased to permit large mass loading of electrochemically active material per unit area and the development of new electrode materials. Traditional planar or two-dimensional (2D) electrode design places a limit on the active material mass loading inside a 2D surface, but it can be expanded by using thicker electrodes. The electrode thickness is nevertheless constrained by the following factors: risks of a thick electrode detaching from the current collector during repeated charge-discharge cycles; slow diffusion/charge and mass transfer of lithium-ion (Li^+) through a thick electrode layer; and, in the case of lithium (Li) metal-based batteries, the electrode's development of Li dendrites, which can short-circuit the battery [28,29]. Three-dimensional (3D) batteries concept is a result of solution of these issues and the need to increase the areal capacity of batteries. A highly developed 3D surface allows for a larger amount of active material to be deposited while maintaining a smaller thickness, thus avoiding the challenges associated with a thick electrode [30,31]. Along with these advantages, an in-plane 3D thin electrode configuration can compensate and/or mitigate an electrode's volume variations due to Li^+ insertion and extraction [32]. Fabrication of NiO in the shape of the 3D thin film is a very suitable approach to obtain the nano-structured material with any shape and size.

One of the physical vapor deposition techniques for producing 3D NiO thin film electrodes is the radio frequency (RF) magnetron sputtering. This method offers the benefit of making large area thin films readily, which is suited for industrial applications with the ability to sputter both conducting and non-conducting materials. Since RF sputtering often takes place under low pressure, there are very few sources of contamination. This guarantees that this technology can be used to create films of high quality.

To ensure the construction of a dense in-plane structure of NiO, the material can be delivered to the expanding surface layer in equal amounts by RF sputtering.

In this paper, in-plane NiO thin film electrodes were deposited via RF magnetron sputtering using the appropriate masks. The post-annealing was used in order to improve the film quality with reduced roughness and better crystalline properties of the NiO [33]. The in-plane 3D microbattery with a GPE that displayed stable cycling performance up to 60 cycles with capacity retention of 94% and CE of 97%. The results showed that the improved performance of the 3D in-plane electrodes are largely attributed to its substantial surface area, the uniform diffusion of Li^+ facilitated by the GPE, and the improved crystallinity of the electrodes.

2. Experimental part

2.1. Material preparation

The sputtering masks were produced using a Laser Scribing Machine (STJ-60FM, STYLECNC). The maximum average laser frequency and the maximum current were 15 kHz 10.9 A, respectively. The laser pulse duration can be varied ranging from 330 fs up to 10 ps. The laser structuring process was performed for achieving masks by applying laser treatment speed of 500 mm/s and laser pulse duration of 350 fs. Electrodes obtained by magnetron sputtering should ideally possess the same shape as the pattern of the mask. Therefore, an important aspect are the edges of

the mask, which are cut in a straight line to obtain well-defined dimensions of the 3D. The laser structuring process was carried out under ambient air and the ablated material was removed by an exhaust.

With the use of the prepared masks, Cr/Pt were sputtered as the first current collector layers. Then the NiO thin films were sputtered via RF reactive magnetron sputtering in the atmosphere of Ar/O_2 at room temperature. Nickel sputtering target (Angstrom Engineering, 99.99% purity, 2" diameter × 0.020" thick) was used as the sputtering source. The sputtering chamber was evacuated down to 2×10^{-6} Torr by a turbo vacuum pump. Argon gas was introduced into the chamber, and pressure was balanced to 5 mTorr. The target was cleaned by a 20 min pre-sputtering before the substrate shutter was removed, in order to eliminate oxide layer and other contaminations on the target surface. Then the sputtering and depositing process lasted for 17 h, leading to an average total thickness of 623.4 nm of active materials on a substrate. As the substrates Si wafer, SS spacers and glass slides were used to investigate SEM images, to test the electrochemical performance in the coin cells and to fabricate 3D microbattery, respectively.

After sputtering thermal annealing was carried out for 10 min at 200, 250, and 300 °C in air. The active mass was determined by calculating the mass difference before and after magnetron sputtering. This method ensured accurate quantification of the active mass in each case. The active mass for the sample NiO before annealing was around 0.040 mg while after annealing at 300 °C it was around 0.045 mg. The NiO thin film can absorb oxygen from the surrounding atmosphere while annealing. This might result in the formation of additional oxide layers, contributing to a modest increase in mass.

Thermal evaporation method was chosen as the preferred method to deposit lithium films. The average thickness of the lithium films was 1 μm.

Poly(ethylene oxide)-poly(vinylidene fluoride-co-hexafluoropropylene) (PEO-PVDF-co-HFP) membranes were used as separators. Polyvinylidene fluoride-co-hexafluoropropylene (PVDF-co-HFP) was selected as a polymer with stable interfacial contact with an electrode. A solution of PVDF-co-HFP (3 wt%) was prepared by dissolving it in Acetonitrile (Sigma Aldrich Chemie GmbH, Steinheim, Germany). The solution was stirred well and heated continuously at 60 °C for 12 h. Polyethylene oxide (PEO) was utilized as a host matrix/gelating agent. Finally, PEO-PVDF-co-HFP solution was prepared by dissolving PEO (2 wt%) in prepared solution with vigorous stirring at 80 °C for several hours until the mixture turned into a homogeneous viscous solution.

Fig. 1 shows step-by-step assembly of NiO-based 3D microbattery with in-plane set-up. First, current collectors of Cr–Pt (5–50 nm) were deposited through maks on the glass substrate, then NiO was sputtered from Ni sputtering target at the following deposition conditions: 75 W, 5 mTorr ($Ar:O_2$ = 1:2) and post-annealed in muffle oven at 300 °C for 10 min. Afterwards, through the second part of the mask Li (1.5 μm) was thermally evaporated using a Thermal Evaporation System (Angstrom Engineering).

2.2. Materials characterization

The crystal structures of the obtained NiO electrodes were analyzed using X-ray diffraction (XRD, SmartLab, Rigaku Co., Japan, Cu Kα radiation, λ = 0.154056 nm). The XRD data were obtained over a 2θ range from 10 to 80 °C at a scan rate of 5°/min using 40 kV, 30 mA X-ray. Scanning electron microscopy (SEM, ZEISS Crossbeam 540, Carl Zeiss AG, Wetzlar, Germany) was employed to investigate the morphology of thin film NiO electrodes. The structure of GPE was analyzed using fourier-transform infrared spectroscopy (FTIR, Nicolet iS10 FT-IR Spectrometer, USA).

2.3. Electrochemical investigation

The electrochemical performance of thin film NiO electrodes was investigated using the CR2032-type coin cells, assembled in an Ar filled glove box (M. Braun Inertgas-Systeme GmbH, Gerlingen, Germany). Metal lithium was used as both counter and reference

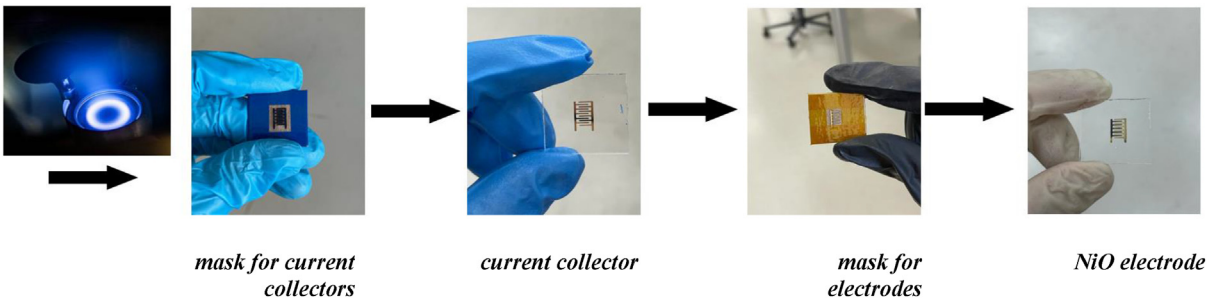

Fig. 1. Step by step of fabrication of in-plane separator-free 3D NiO-based lithium-metal microbattery.

electrodes. A Celgard 2400 microporous polypropylene and PEO-PVDF-co-HFP membranes were used as separators. The electrolyte was 3–4 drops of 1 M $LiPF_6$ in a mixture of ethylene carbonate/ethyl-methyl carbonate/dimethyl carbonate (EC/EMC/DC, 1:1:1 vol %).

The coin cells were tested galvanostatically on a multi-channel battery testing system (BT-2000, Arbin Inc., and Neware Battery tester, Neware Co.) at a current density of 0.1C, between the cutoff potentials 0.01 and 3V. Cyclic voltammetry (CV) and electrochemical impedance spectroscopy (EIS) were performed using a VMP3 potentiostat/galvanostat (Bio-Logic Science Instrument Co.). CV was carried out at the scan rate of 0.1 mV s^{-1} between 0.01 V and 3 V range. EIS was performed to determine charge transfer resistance of electrodes. To measure the impedance of uncycled coin-cells, the coin cells were first cycled three times to activate the anode with the consequent resting time for 5 h. The impedances of the cycled electrodes were recorded at a frequency range from 0.1 Hz to 100 kHz with the altering voltage signal of 10 mV.

3. Results and discussions

The deposited in-plane 3D NiO thin films were annealed in a muffle furnace in air at 200–300 °C for 10 min in order to improve the crystallinity and the adhesion of the thin film to the substrate. The heating rate was 5 °C/min. The sputtered NiO electrodes were characterized using X-ray diffraction (XRD) analysis in order to identify the phases present. For comparison, Fig. 2 shows the XRD patterns for as-deposited and thermally treated NiO at 200–300 °C for 10 min. The diffraction patterns indicate the successful formation of NiO on the substrate. The NiO has three sharp peaks situated at 2θ = 37.20, 44.80, and 64.30, which correspond to the (111), (200), and (200) crystal planes of rhombohedral NiO. No other diffraction peaks were detected, indicating that pure NiO was formed without any other impurity phase.

The observed shifts in the peaks of thin film NiO, corresponding to an increase in annealing temperature, can be attributed to thermal-induced modifications in the material's structural and compositional characteristics. Elevated annealing temperatures augment atomic mobility, prompting changes in crystal lattice parameters, grain boundaries, and lattice strain, thereby influencing the XRD pattern.

Fig. 3 presents the SEM images of the 3D thin film as-deposited NiO anodes and after annealing at 200–300 °C. Cross-SEM images show the thicknesses of the sputtered NiO anodes before and after heat

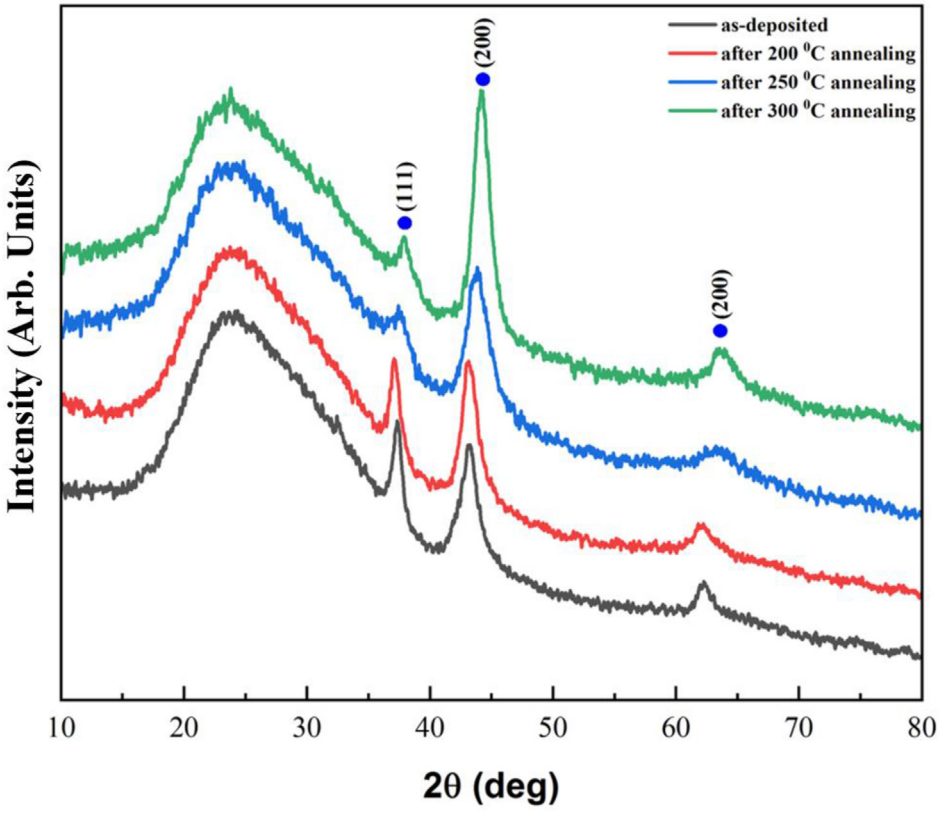

Fig. 2. XRD patterns of thin film NiO before and after thermally oxidation at 200–300 °C.

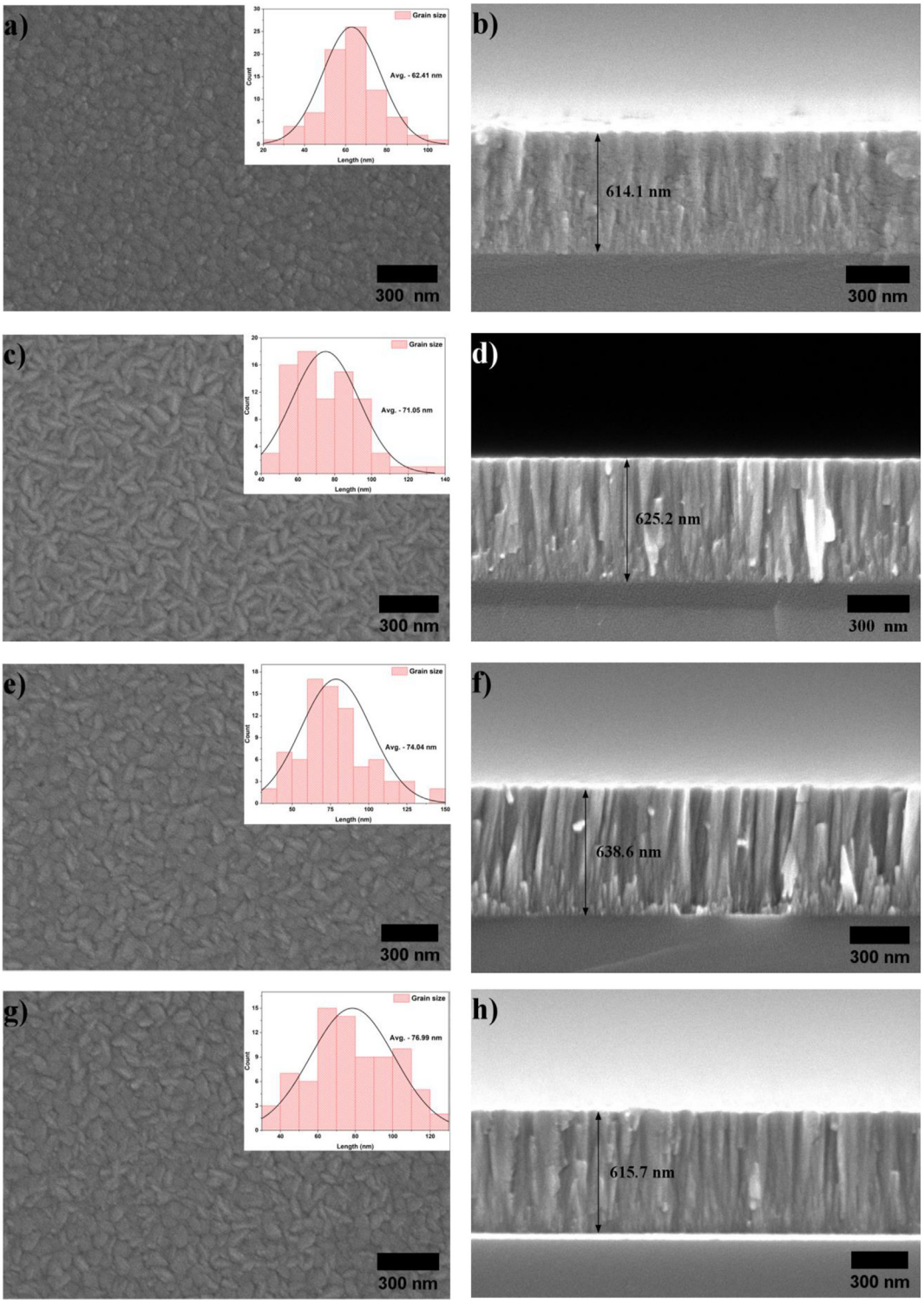

Fig. 3. Surface and cross-sectional SEM images of 3D thin film as-deposited NiO anodes (a,b) and after annealing at 200 °C (c,d), 250 °C (e,f), 300 °C (g,h).

treatment ranging from 614.1 to 638.6 nm. Surface SEM images of NiO electrodes after annealing reveal minor microstructural changes. It was observed that grain boundaries increased slightly with increasing temperature. It is noteworthy that all the electrodes exhibit an absence of discernible cracks and defects. The augmentation of grain boundaries in the annealed NiO electrodes can be attributed to thermally induced

crystallization and diffusion processes, prompting the formation of larger and more well-defined crystalline structures. Larger grain sizes and well-defined crystalline structures are conducive to improved charge transport and lithium-ion diffusion within the electrode material. Consequently, these microstructural enhancements may positively impact the electrode's capacity, and cycling stability. The thickness of the NiO film varies with annealing temperature due to processes of grain growth and densification. At moderate annealing temperatures, grain growth and crystallization increase the film thickness slightly as grains form and expand. However, at higher temperatures, further annealing at 300 °C may lead to densification, where the grains pack more tightly, reducing porosity and compacting the film. This structural compaction causes a decrease in the overall thickness of the NiO film (Fig. 3h).

FTIR results confirm the presence of polymers PEO and PVDF-co-HFP layer after coating (Fig. 4). The resulting spectra have typical peaks of PVDF α and β phases, which appear at 1398.7 cm^{-1} and 833.5 cm^{-1}, respectively. The peak at 1234.4 cm^{-1} refers to the C–F of PVDF stretching frequency. Peaks at 1166.3 cm^{-1} and 1069.8 cm^{-1} correspond to C–O–C stretching, C–H stretching is observed at 2878.3 cm^{-1} of PEO. The allowed modes of vibration of various functional groups of PEO and PVDF correspond to the observed IR characteristic bands of polymer blend film which confirm the presence of PEO and PVDF.

To analyze lithiation/delithiation reactions of NiO electrodes, CV tests were conducted between 0.01 and 3.0 V (versus Li/Li^+) at a scanning speed of 0.1 mV s^{-1}. Fig. 5 shows CV curves of an as-deposited NiO electrode and after annealing at different temperatures. A sharp reduction peak emerged at ~0.76 V in the first discharge process, corresponding to the reaction $NiO + 2Li^+ + 2e^- \rightarrow Ni + Li_2O$. In the subsequent cycles, the peak became weaker and split into two peaks located at ~0.73 V (denoted as R_1) and ~1.2 V (denoted as R_2), corresponding to reactions $NiO + Li^+ + e^- \rightarrow 0.5Li_2NiO_2 + 0.5Ni$ and $0.5Li_2NiO_2 + Li^+ + e^- \rightarrow 0.5Ni + 2Li_2O$, respectively. In the charge processes, two oxidation peaks at ~1.42 V (denoted as O_2) and ~2.3 V (denoted as O_1) can be detected and associated with the reactions $0.5Ni + Li_2O - e^- \rightarrow 0.5Li_2NiO_2 + Li^+$ and $0.5Ni + 0.5Li_2NiO_2 - e^- \rightarrow NiO + Li^+$, respectively. CV curves of all the NiO electrodes non annealed and annealed at the temperature range of 200–300° show no essential differences [34]. The initial cathodic peak between approximately 0.35–0.85 V during the first cycle is attributed to the formation of amorphous Li_2O, the formation of a solid

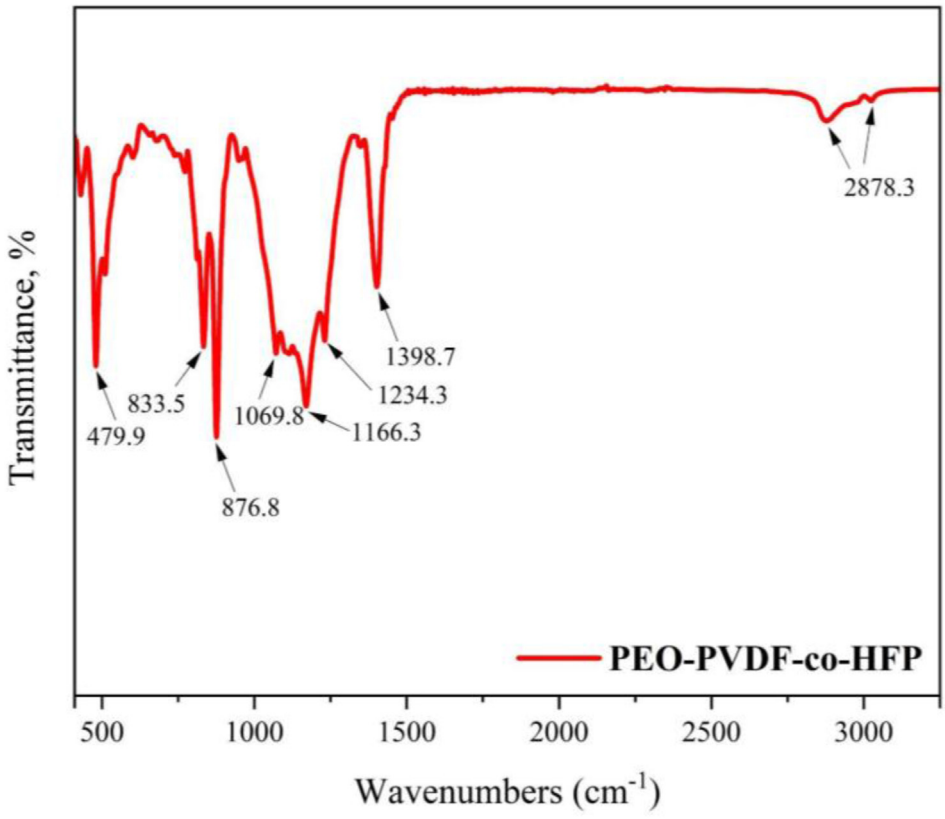

Fig. 4. FTIR spectra for NiO with PEO-PVDF-co-HFP.

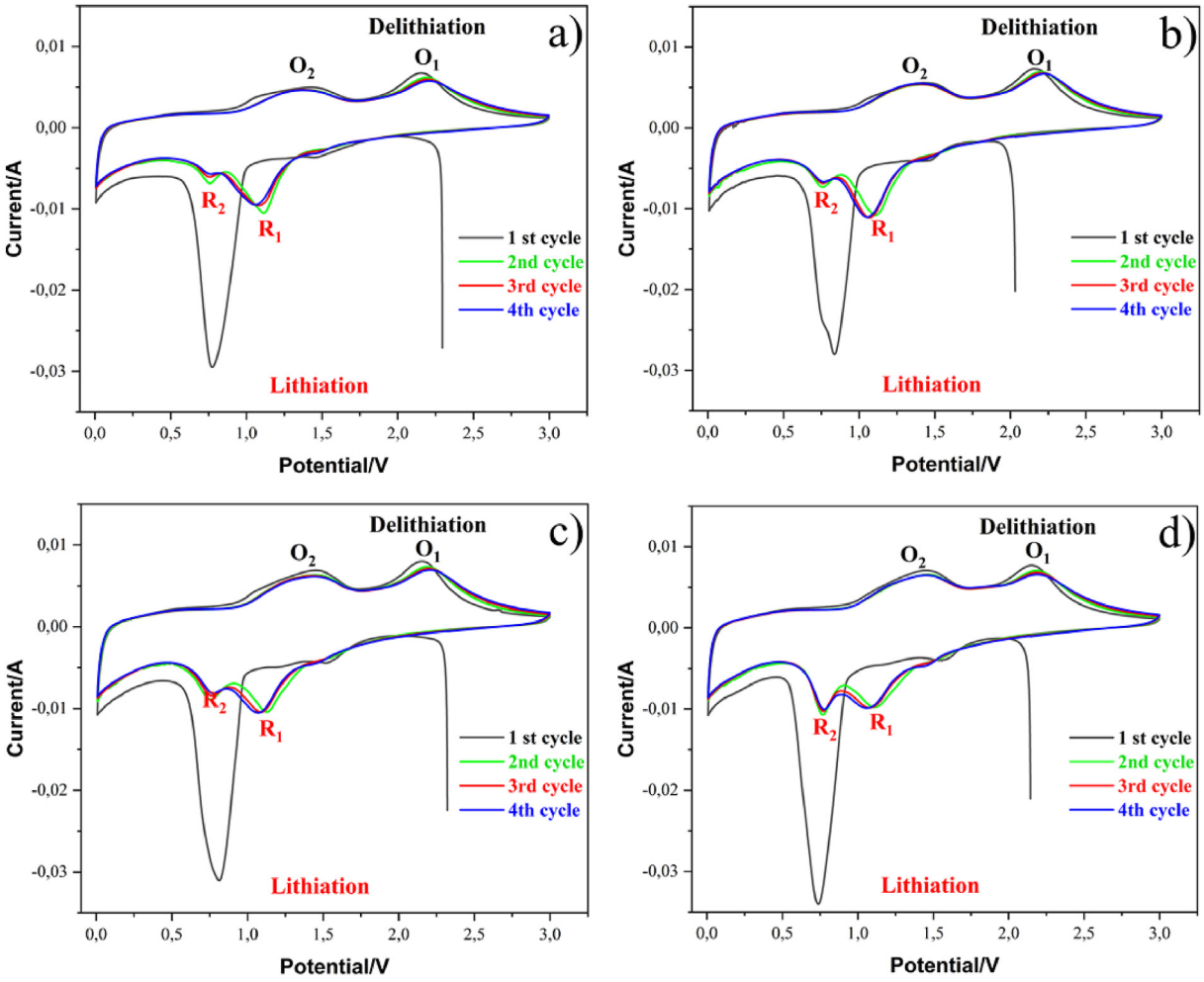

Fig. 5. Cyclic voltammograms of 3D thin film as-deposited NiO anodes and after annealing at 200–300 °C (with Celgard separator).

electrolyte interphase (SEI) film, and the reduction of NiO to Ni.

Fig. 6 displays the comparative cycling performance of the as-deposited NiO (Fig. 4a) and annealed at different temperatures 200, 250, and 300 °C (Fig. 4b–d) at a 0.1 C rate in the voltage range of 0.01–3.0 V. The capacity of thin film as-deposited NiO electrode and annealed at 200, 250, and 300 °C is about 500 mAh g^{-1}, 505 mAh g^{-1}, 590 mAh g^{-1} and 600 mAh g^{-1}, respectively, with approximately 90% of CE. Then increase gradually can be observed till the 20th cycle due to the poor ionic conductivity of PVA and PAN. It can be noted that the cell with NiO annealed at 300 °C had constant CE. Starting from the 2nd cycle, CE of all samples became stable, but for the sample annealed at 300 °C, it was higher - 100%, indicating the better performance in comparison with as-deposited cells and after heat treatment.

Afterwards, the cell with the best performance (Fig. 5d) has been tested with the PEO-PVDF-co-HFP GPE at the same conditions. Fig. 6e represents the cycle performance of prepared thin film NiO electrodes annealed at 300 °C. Initially, the cyclic performance of the cell was studied at a current density of 0.1C. Compared with the same electrode but cycled with a Celgard separator, we can see that the capacity had an more expressed increasing trend and reached approximately the same values of the capacity by the 25th cycle. The charge and discharge capacities maintain 579 mAh g^{-1} and 901 mAh g^{-1} during the 1st cycle, respectively. At the 60th cycle the capacity remained at the level of 510 mAh g^{-1} and with approximately 98% CEs. Slightly lower values of capacities for the same electrodes but different electrolytes can be ascribed to the lower ionic conductivity of PEO and PVDF. Fig. 6f shows the discharge-charge curves of thin film NiO electrodes annealed at 300 °C in the initial 5 cycles and at the 10th cycle. The charge and discharge plateaus on the galvanostatic charge/discharge curves are in good consistency with the CV results. The initial discharge

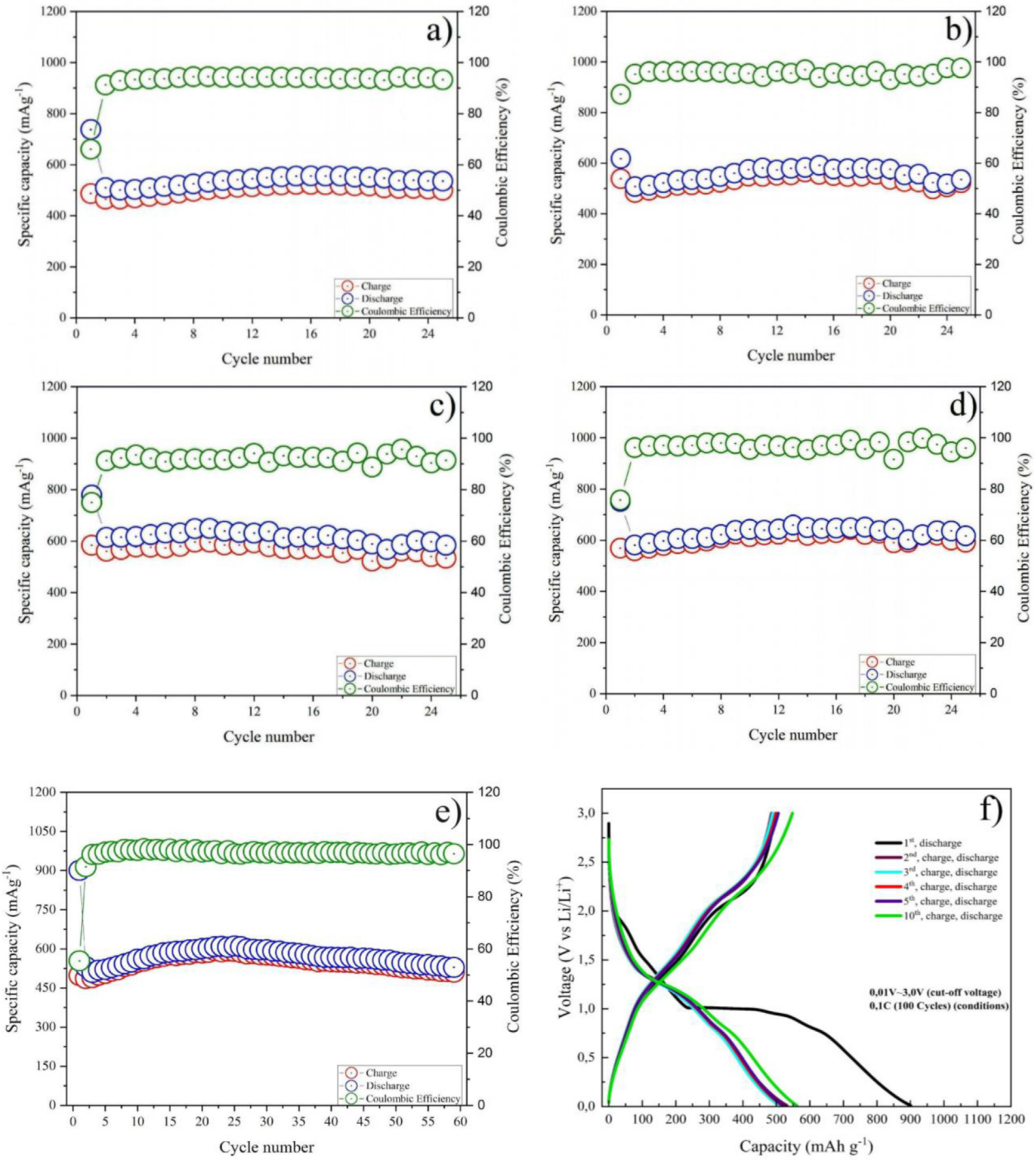

Fig. 6. Cycle performance of 3D thin film as-deposited NiO anodes (a) and after annealing at 200 °C (b), 250 °C (c), 300 °C (d) (with Celgard separator), cycle performance (e) and charge-discharge curves (f) of 3D thin film NiO anodes annealed at 300 °C (with PEO-PVDF-co-HFP GPE).

plateau of the NiO electrode is located at around ~0.7 V, which is in the middle of potential range for the SEI formation (0.5—0.7 V). Hence the formation of SEI is accompanied by drastic volume expansion throughout the initial lithiation of NiO. The specific discharge capacity of the as-deposited thin film NiO electrodes remained steady in the 30 cycles, with a retention rate of 96.3% at the 20th cycle versus 60th cycle.

Fig. 7 shows the Nyquist plots of the electrochemical impedance spectra of the 3D thin film NiO anode annealed at 300 °C. After the cycling process, the impedance was determined. Nyquist plot shares the

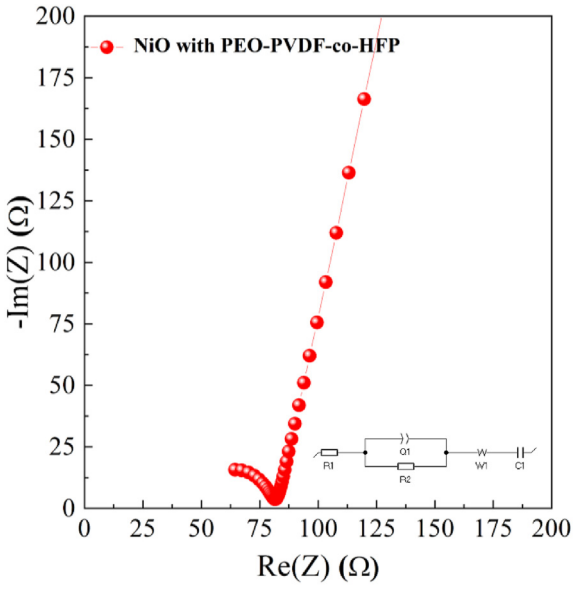

Fig. 7. Nyquist plot of cycled of 3D thin film NiO electrode annealed at 300 °C with the fitted circuit.

same characteristics, including a semicircle in the middle frequency range that is often related with charge transfer and an inclined line in the low frequency range that is responsible for lithium ion diffusion in the majority of the electrode. The circuit components of R_1, R_2, Q_1, W_1, and C_1 represent the NiO@PEO-PVDF-co-HFP, SEI resistance, charge transfer impedance, diffusion-controlled Warburg impedance, and capacitance, respectively. According to the results of the fitted equivalent circuit, the charge transfer resistances of the electrode was measured to be 81.2 Ohm, which is quite higher than for NiO@PEO as it was reported in recent work by Arinova et al. [35]. The higher charge transfer resistance of the NiO@PEO-PVDF-co-HFP compared to NiO@PEO can be explained by the potentially lower ionic conductivity of PVDF-co-HFP.

Finally, the cell with 3D NiO thin film electrode annealed at 300 °C was assembled in a glovebox in the Ar atmosphere. At first, a Cu current collector was connected at the tail of the electrodes using silver paste. Furthermore, PEO-PVDF-co-HFP polymer was introduced on the electrodes. The polymer film on the surface of the electrodes was activated by adding 2–3 drops of 1 M $LiPF_6$ electrolyte solution of EC, EMC and DC (1:1:1 (v/v) ratio). A polymeric bag was constructed such as to house the 3D cell and sealed with a pouch sealing machine at 90 °C. A pictorial view of the shapes of the cathode/anode deposited by magnetron and assembled in-plane type 3D microbattery was shown in Fig. 8(a,b). Its nominal voltage was 1.0 V Fig. 8c.

4. Conclusion

In summary, magnetron sputtering and thermal evaporation techniques were employed with using 3D masks to develop in-plane type 3D NiO and Li thin film electrodes for LIBs.

Changes in surface morphology of the thin film NiO electrodes after annealing at 200–300 °C were revealed by SEM. A facile thermal oxidation method allowed obtaining NiO thin film electrodes with improved electrochemical performance. The electrochemical performance of the cell with PEO-PVDF-co-HFP GPE was comparable to the cell with a commercial separator. The cycling stability results displayed an outstanding performance for the NiO annealed at 300 °C with PEO-PVDF-co-HFP GPE, delivering a capacity of 510 mAh g^{-1} at a 0.1 C rate after 60th cycles.

The stated results allowed developing in-plane type 3D cells, which is a promising result for further

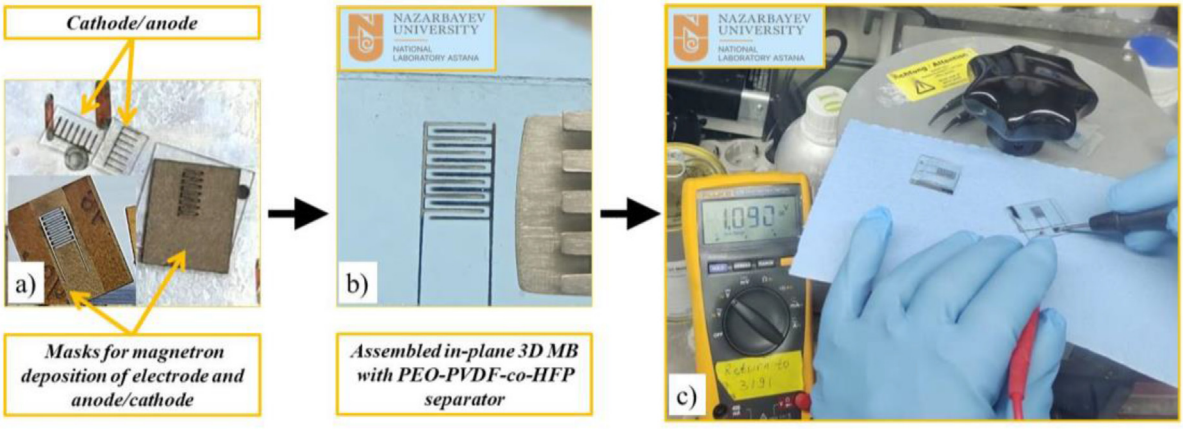

Fig. 8. Pictorial view of fabricated cathode/anode by magnetron sputtering using masks (a), assembled in-plane type 3D microbattery (b), voltage measurement (c).

investigation of high-energy-density thin film 3D batteries.

Funding

The work was funded by the research grant NO AP19680567, AP19578472 and BR21882402 from the Ministry of Science and Higher Education of the Republic of Kazakhstan.

Conflict of interest

The authors declare no conflict of interests.

References

[1] L. Xiao, E. Li, J. Yi, W. Meng, S. Wang, B. Deng, J. Liu, Enhancing the performance of nanostructured ZnO as an anode material for lithium-ion batteries by polydopamine-derived carbon coating and confined crystallization, J. Alloys Compd. 764 (2018) 545, https://doi.org/10.1016/j.jallcom.2018.06.081.

[2] J. Zhao, Y. Zhang, Y. Wang, H. Li, Y. Peng, The application of nanostructured transition metal sulfides as anodes for lithium ion batteries, J. Energy Chem. 27 (2018) 1536, https://doi.org/10.1016/j.jechem.2018.01.009.

[3] H. Su, S. Jaffer, H. Yu, Transition metal oxides for sodium-ion batteries, Energy Storage Mater. 5 (2016) 116, https://doi.org/10.1016/j.ensm.2016.06.005.

[4] Y. Yan, B. Wang, C. Yan, D. Kang, Decorating ZnO nanoflakes on carbon cloth: free-standing, highly stable lithium-ion battery anodes, Ceram. Int. 45 (2019) 15906, https://doi.org/10.1016/j.ceramint.2019.05.097.

[5] J.S. Wei, Z.Y. Zhu, X. Zhao, T.B. Song, J.H. Huang, Y.X. Zhang, L. Chen, X.Q. Niu, Y.G. Wang, H.M. Xiong, Self-assembled ZnO-carbon dots anode materials for high performance nickel-zinc alkaline batteries, Chem. Eng. J. 425 (2021) 130660, https://doi.org/10.1016/j.cej.2021.130660.

[6] Y. Song, Y. Chen, Z. Wang, W. Zhao, C. Qin, H. Yu, X. Wang, Z. Bakenov, Y. Zhang, Defective ZnOx@porous carbon nanofiber network inducing dendrite-free zinc plating as zinc metal anode for high-performance aqueous rechargeable Zn/Na4Mn9O18 battery based on hybrid electrolyte, J. Power Sources 518 (2022) 230761, https://doi.org/10.1016/j.jpowsour.2021.230761.

[7] V.K.H. Bui, T.N. Pham, J. Hur, Y.C. Lee, Review of ZnO binary and ternary composite anodes for lithium-ion batteries, Nanomaterials 11 (2021) 2001, https://doi.org/10.3390/nano11082001.

[8] D. Deckenbach, J.J. Schmeider, A 3D hierarchically porous nanoscale ZnO anode for high-energy rechargeable zinc-air batteries, J. Power Sources 488 (2021) 229393, https://doi.org/10.1016/j.jpowsour.2020.229393.

[9] N. Joshi, L. Silva, F.M. Shimizu, V.R. Mastelaro, J.C. M'Pekoo, L. Lin, O.N. Oliveira Jr., UV-assisted chemiresistors made with gold modified ZnO nanorods to detect ozone gas at room temperature, Microchim. Acta 186 (2019) 418, https://doi.org/10.1007/s00604-019-3532-4.

[10] C.S. Yudha, A.P. Hutama, M. Rahmawati, H. Widiyandari, H. Nursukatmo, H. Nilasary, H.S. Oktaviano, A. Purwanto, Synthesis and characterization of ZnO from thermal decomposition of precipitated zinc oxalate dihydrate as an anode material of Li-ion batteries, Energies 14 (2021) 598шот0, https://doi.org/10.3390/en14185980.

[11] D.K. Shah, D. KC, M.S. Akhtar, C.Y. Kim, O.B. Yang, Vertically arranged zinc oxid-e nanorods as antireflection layer for crystalline silicon solar cell: a simulation study of photovoltaic properties, Appl. Sci. 10 (2020) 6062, https://doi.org/10.3390/app10176062.

[12] F. Zhang, B. Wang, Y. Shen, Blue luminescent ZnO nanoclusters stabilized by esterifiable polyamidoamine dendrimers and their UV-shielding applications, Asian J. Chem. 26 (2014), https://doi.org/10.14233/ajchem.2014.15942.

[13] Z. Han, Y. Li, F. Chen, S. Tang, P. Wang, Preparation of ZnO/Ag2O nano-fibers by coaxial electrospinning and study of their photocatalytic properties, Chem. J. Chin. Univ. Chin. 41 (2020) 308–316.

[14] Z.Y. Han, Y.J. Li, X. Lin, Z.Y. Wang, Z.Q. Li, H. Wang, Preparation and photoelectrocatalytic performance of Fe2O3/ZnO composite electrode loading on conductive glass, Chem. Res. Chin. Univ. 39 (2018) 771–778, https://doi.org/10.1007/s12613-020-2096-y.

[15] S. Chen, S. Zhou, J. Fu, S. Tang, X. Wu, P. Zhao, Z. Zhang, A near infrared fluorescence imprinted sensor based on zinc oxide nanorods for rapid determination of ketoprofen, Anal. Methods 13 (2021) 2836–2846, https://doi.org/10.1039/D1AY00555C.

[16] V. Bhati, S. Ranwa, M. Fanetti, M. Valant, M. Kumar, Efficient hydrogen sensor based on Ni-doped ZnO nanostructures by RF sputtering, Sensor. Actuator. B Chem. 255 (2018) 588, https://doi.org/10.1016/j.snb.2017.08.106.

[17] K. Joshi, M. Rawat, S. Gautam, R. Singh Ramola, F. Singh, Band gap widening and narrowing in Cu-doped ZnO thin films, J. Alloys Compd. 680 (2018) 252–258, https://doi.org/10.1016/j.jallcom.2016.04.093.

[18] J. Yuan, X. Zhang, C. Chen, Y. Hao, R. Agrawal, C. Wang, W. Li, H. Yu, Y. Yu, X. Zhu, et al., Facile fabrication of three-dimensional porous ZnO thin films on Ni foams for lithium ion battery anodes, Mater. Lett. 190 (2017) 37, https://doi.org/10.1016/j.matlet.2016.12.126.

[19] E. Quartarone, V. Dall'Asta, A. Resmini, C. Tealdi, I.G. Tredici, U. A. Tamburini, P. Mustarelli, Graphite-coated ZnO nanosheets as high-capacity, highly stable, and binder-free anodes for lithium-ion batteries, J. Power Sources 320 (2016) 314, https://doi.org/10.1016/j.jpowsour.2016.04.107.

[20] D. Wang, J. Guo, C. Cui, J. Ma, A. Cao, Controllable synthesis of CNT@ZnO composites with enhanced electrochemical properties for lithium-ion battery, Mater. Res. Bull. 101 (2018) 305, https://doi.org/10.1016/j.materresbull.2018.01.052.

[21] Y. Li, Y. Huang, X. Wang, W. Liu, K. Yu, C. Liang, Simple synthesis of rice husk hollow carbon-coated flower ZnO for the anode in a high performance lithium-ion battery, J. Phys. Chem. Solid. 145 (2020) 109540, https://doi.org/10.1016/j.jpcs.2020.109540.

[22] M. Armand, J.-M. Tarascon, Building better batteries, J. Nature 451 (2008) 652–657, https://doi.org/10.1038/451652a.

[23] N.-S. Choi, Z. Chen, S.;A. Freunberger, X. Ji, Y.-K. Sun, K. Amine, G. Yushin, L.F. Nazar, J. Cho, P.G. Bruce, Challenges facing lithium batteries and electrical double-layer capacitors, J. Angew. Chem. Int. Ed. 51 (2012) 9994–10024, https://doi.org/10.1002/anie.201201429.

[24] B. Scrosati, J. Hassoun, Y.-K. Sun, Lithium-ion batteries. A look into the future, J. Energy Environ. Sci. 4 (2011) 3287–3295, https://doi.org/10.1039/c1ee01388b.

[25] G.E. Blomgren, The development and future of lithium ion batteries, J. Electrochem. Soc. 164 (2017) 5019–5025, https://doi.org/10.1149/2.0251701jes.

[26] S. Ferrari, M. Loveridge, S.D. Beattie, M. Jahn, R.J. Dashwood, R. Bhagat, Latest advances in the manufacturing of 3D rechargeable lithium microbatteries, J. Power Sources 286 (2015) 25–46, https://doi.org/10.1016/j.jpowsour.2015.03.133.

[27] A. Mentbayeva, S. Sukhishvili, M. Naizakarayev, N. Batyrgali, Ultrathin clay-containing layer-by-layer separator coating enhances performance of lithium-sulfur batteries, J. Electrochim. Acta 366 (2021) 137454, https://doi.org/10.1016/j.electacta.2020.137454.

[28] C. Fongy, A.-C. Gaillot, S. Jouanneau, D. Guyomard, B. Lestriez, Ionic vs electronic power limitations and analysis of the fraction of wired grains in LiFePO [sub 4] composite electrodes, J. Electrochem. Soc. 157 (2010) A885, https://doi.org/10.1149/1.3432559.

[29] P.V. Braun, J. Cho, J.H. Pikul, W.P. King, H. Zhang, High power rechargeable batteries, J. Curr. Opin. Solid State Mater. Sci. 16 (2012) 186–198, https://doi.org/10.1016/j.cossms.2012.05.002.

[30] G.E. Blomgren, The development and future of lithium ion batteries, J. Electrochem. Soc. 164 (2017) A5019—A5025, https://doi.org/10.1149/2.0251701jes.
[31] A. Nurpeissova, A. Adi, A. Aishova, A. Mukanova, S.S. Kim, Z. Bakenov, Synergistic effect of 3D current collector structure and Ni inactive matrix on the electrochemical performances of Sn-based anodes for lithium-ion batteries, Mater. Today Energy 16 (2020) 100397, https://doi.org/10.1016/j.mtener.2020.100397.
[32] T.S. Arthur, D.J. Bates, N. Cirigliano, D.C. Johnson, P. Malati, J. M. Mosby, E. Perre, M.T. Rawls, A.L. Prieto, B. Dunn, Three-dimensional electrodes and battery architectures, J. MRS Bull. 36 (2011) 523—531, https://doi.org/10.1557/mrs.2011.156.
[33] J. Husna, Aliyu M. Mannir, Islam M. Aminul, P. Chelvanathan, Hamzah N. Radhwa, M. Sharafat Hossain, M.R. Karim, N. Amin, Influence of annealing temperature on the properties of ZnO thin films grown by sputtering, J. Energy Procedia 25 (2012) 55—61, https://doi.org/10.1016/j.egypro.2012.07.008.
[34] Q. Zheng, Y. Liu, H. Guo, et al., Synthesis of hierarchical 1D NiO assisted by microwave as anode material for lithium-ion batteries, Mater. Res. Bull. 98 (2018) 155—159, https://doi.org/10.1016/j.materresbull.2017.10.017.
[35] A. Arinova, G. Kalimuldina, A. Nurpeissova, Z. Bakenov, Electrophoretic deposition of poly(ethylene oxide) gel-polymer electrolyte for 3D NiO/Ni foam anode based lithium-ion batteries, J. Electrochem. Soc. 170 (2023) 100501, https://doi.org/10.1149/1945-7111/acfe3e.